Weak ferromagnetic order breaking the threefold rotational symmetry of the underlying kagome lattice in CdCu$_3$(OH)$_6$(NO$_3$)$_2 \cdot$ H$_2$O

Ryutaro Okuma, Takeshi Yajima, Daisuke Nishio-Hamane, Tsuyoshi Okubo, and Zenji Hiroi

Institute for Solid State Physics, University of Tokyo, Kashiwa, Chiba 277–8581, Japan

Novel magnetic phases are expected to occur in highly frustrated spin systems. Here, we study the structurally perfect kagome antiferromagnet CdCu$_3$(OH)$_6$(NO$_3$)$_2 \cdot$ H$_2$O by magnetization, magnetic torque, and heat capacity measurements using single crystals. An antiferromagnetic order accompanied by a small spontaneous magnetization that surprisingly is confined in the kagome plane sets in at $T_N \sim 4$ K, well below the nearest-neighbor exchange interaction $J/k_B = 45$ K. This suggests that a unique "$\mathbf{q} = 0$" type 120° spin structure with "negative" (downward) vector chirality, which breaks the underlying threefold rotational symmetry of the kagome lattice and thus allows a spin canting within the plane, is exceptionally realized in this compound rather than a common one with "positive" (upward) vector chirality. The origin is discussed in terms of the Dzyaloshinskii-Moriya interaction.

I. INTRODUCTION

Highly frustrated antiferromagnets with triangle-based lattices have been extensively studied both theoretically and experimentally, lured by a fascinating conjecture that the geometrical frustration enforces spins to disorder even at low temperatures and realizes exotic ground states defeating the conventional Néel order. In particular, strong frustration in kagome antiferromagnets (KAFMs) with nearest-neighbor magnetic interactions J in the kagome net made of corner-sharing triangles has been focused on because it should result in macroscopic degeneracy in the ground state of the classical Heisenberg model [1–4], while, for the spin-1/2 Heisenberg model, one expects Z_2 gapped or gapless U(1) Dirac quantum spin-liquid states induced by large quantum fluctuations [5,6]. However, these exotic ground states are elusive and tend to be superseded by certain noncollinear long-range orders (LROs). Nevertheless, the KAFM is intriguing as it may exhibit an unconventional LRO with an emerging chiral degree of freedom on every triangle. The chirality is an important ingredient to recent condensed matter physics because it can generate topological spin textures such as skyrmions [7] and may couple with lattice, polarization, and conduction electrons in various ways to generate novel phenomena [8,9].

There are often additional interactions that may transform spin-liquid states into LROs in the spin-1/2 KAFM, which are interplane couplings, further-neighbor interactions, exchange anisotropy, Dzyaloshinskii-Moriya (DM) interaction, and so on. For example, the DM interaction prefers a coplanar $\mathbf{q} = 0$ order [Figs. 1(a) and 1(b)] when its magnitude is larger than 10% of J [10]. On the other hand, ferromagnetic second-neighbor interactions favor the $\mathbf{q} = (1/3\ 1/3)$ order [Fig. 1(c)], and, further-neighbor interactions may stabilize more complex, noncoplanar spin structures with larger unit cells such as the 12-sublattice order called the cuboc order [11].

The three coplanar 120° structures illustrated in Fig. 1 are distinguished by the vector chirality κ defined for each triangle by Eq. (1):

$$\kappa = \frac{2}{3\sqrt{3}}(S_1 \times S_2 + S_2 \times S_3 + S_3 \times S_1). \quad (1)$$

Following the convention that the spins in the cross products appear rotating counterclockwise around the triangle, as shown in Fig. 1(a), the vector chirality points up and down normal to the kagome plane in every triangle for Figs. 1(a) and 1(b), respectively, while is staggered in Fig. 1(c). Let us call the up and down κ as "positive" and "negative," respectively, as widely used. Then, we call the three types of spin structures with different arrangements of κ "positive" vector chirality (PVC), "negative" vector chirality (NVC), and staggered vector chirality (SVC) structures, respectively.

Among these three structures, the PVC order has been often observed in actual compounds. The $S = 5/2$ Fe jarosite KFe$_3$(OH)$_6$(SO$_4$)$_2$ exhibits a PVC order at 65 K [12,13], while vesignieite, which is a structurally perfect or a slightly distorted $S = 1/2$ KAFM [14,15], seems to show a PVC order at 9 K [16]. A PVC-type order with $\langle 100 \rangle$ anisotropy is also reported in quinternary oxalate compounds with a distorted kagome lattice comprising Fe^{2+} [17]. On the other hand, a SVC order appears at 6 K in herbertsmithite, which is a structurally perfect $S = 1/2$ KAFM comprising $d(x^2 - y^2)$ orbitals of Cu^{2+} ions [18] and seems to have a gapped spin-liquid state [19], when pressure above 2.5 GPa is applied [20]. In contrast, to our knowledge, there is no example of the NVC order for localized spin systems and thus has been rarely studied. The notable feature of NVC is that it loses all threefold rotation axes present in the underlying kagome lattice unlike PVC or SVC. Therefore, it is intriguing to search for a KAFM that exhibits an NVC structure, which would provide us with a chance to study the property of this unusual magnetic order.

In this study, we focus on CdCu$_3$(OH)$_6$(NO$_3$)$_2 \cdot$ H$_2$O [21] which is to be called Cd-kapellasite (CdK) for short. CdK is isostructural to kapellasite, ZnCu$_3$(OH)$_6$Cl$_2$ [22]: compared to kapellasite, Cd^{2+} and NO$_3^-$ ions are substituted for Zn^{2+} and Cl$^-$ ions, respectively, and additional H$_2$O is intercalated in CdK (Fig. 2). CdK crystallizes in a trigonal structure with space group $P\bar{3}m1$ and lattice constants of $a = 6.522$ Å and $c = 7.012$ Å. There is a single Cu site which forms a Cu(OH)$_4$(NO$_3$)$_2$ octahedron heavily elongated toward the apical NO$_3^-$ ions by the Jahn-Teller effect. Thus, the $d(x^2 - y^2)$ orbital takes the highest d level of the Cu^{2+} ion and accommodates spin 1/2. The Cu(OH)$_4$(NO$_3$)$_2$ octahedra
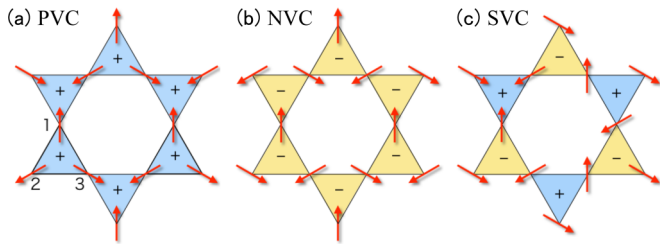
FIG. 1. Three coplanar 120° spin structures. A spin on each lattice point is represented by an arrow, and the direction of the vector chirality on each triangle is shown by "+" (up) or "−" (down). The two $\mathbf{q} = 0$ type structures, "positive" vector chirality (PVC) and "negative" vector chirality (NVC) structures, are shown in (a) and (b), respectively, and the $\sqrt{3} \times \sqrt{3}$ structure with $\mathbf{q} = (1/3\ 1/3)$, a staggered vector-chirality (SVC) structure, in (c). The numbers around the lower-left triangle of (a) refer to those in Eq. (1).

form a kagome layer that contains an undistorted kagome net of spin 1/2, as in herbertsmithite, with the Cd atom located at the center of the hexagon. The nitrate ions and water molecules separate the kagome layers with an interplane distance as long as 7.012 Å, which is larger than 5.733 Å for kapellasite and is much larger than ~ 2 Å in the plane, indicating a good two dimensionality in magnetic interactions. There is one possible source of crystallographic disorder in CdK, which is associated with the configuration of the $NO_3{}^-$ unit [21].

On the magnetic properties of CdK, the previous studies using polycrystalline samples found relatively large, antiferromagnetic Weiss temperatures of $\Theta_W = -114 \pm 27$ K [23] or -62 K [24]. A magnetic LRO is observed at $T_N = 4 \sim 5$ K, which is accompanied by a weak ferromagnetism. The large frustration factor of $\Theta_W/T_N > 15$ indicates a presence of significant magnetic frustration. In contrast, kapellasite and its Mg analog, haydeeite, have nearly zero Weiss temperatures, suggesting that competing ferromagnetic and antiferromagnetic interactions largely compensate each other [25]. They exhibit no LRO above 2 K and a weak ferromagnetic order at 4 K, respectively. However, detailed magnetic properties, spin

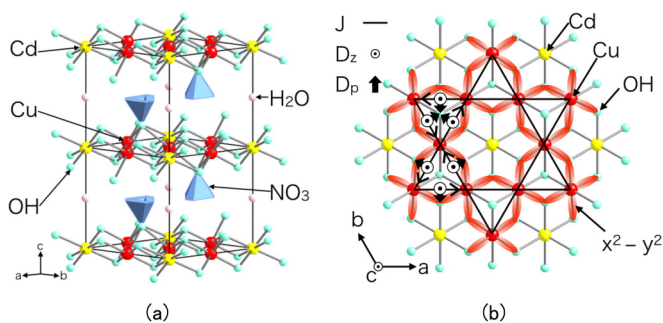FIG. 2. Crystal structures of $CdCu_3(OH)_6(NO_3)_2 \cdot H_2O$ (CdK) (a) and the kagome layer viewed along the [001] direction (b) [21]. In (b), the arrangement of $d(x^2 - y^2)$ orbitals is depicted by the red lobes. The nearest-neighbor magnetic exchange interactions are shown by the thick lines. D_z and D_p in the pair of triangles represent the out-of-plane and in-plane components of the DM vector, respectively. The arrows on the pair of triangles represent the rotational direction in the cross products of the DM interactions, which is always counterclockwise.
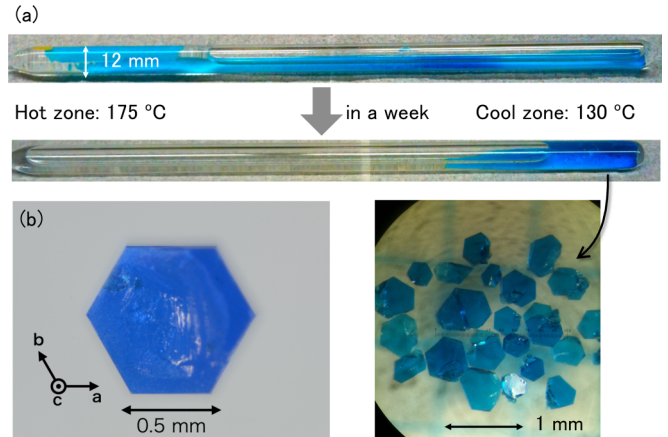

FIG. 3. (a) Crystal growth by the hydrothermal transport method and grown crystals. (b) Crystal of CdK used in the present experiments.

structures, and the origin of LRO are not known partly because of the lack of single-crystalline samples.

In this study, we have synthesized single crystals of CdK and performed magnetization and heat capacity measurements, which suggest that a NVC order is realized in CdK.

II. EXPERIMENT

Single crystals of CdK were synthesized by the hydrothermal transport method similar as used for the single-crystal growth of herbertsmithite [26]. 5 g of $Cd(NO_3)_2 \cdot 4H_2O$ (98%, Sigma-Aldrich), 0.1 g of $Cu(OH)_2$ (90%, Wako Chemical), and 4 ml of deionized water were put into a quartz ampoule of 250 mm long and 12 mm in diameter, as shown in Fig. 3(a). Then, the ampoule was heated in a transparent furnace having a temperature gradient between 130 °C and 175 °C for a week. Light-blue precipitates first spreading over the ampoule were gradually transported to the cool zone, and many hexagonal blue crystals were finally obtained. The crystal of 0.5 mm both in edge and height shown in Fig. 3(b) was picked up and further examined.

A powder x-ray diffraction (XRD) pattern from crushed crystals was in good agreement with the calculated pattern, indicating that there is no impurity inclusion. Single-crystal XRD results are consistent with the $P-3m1$ structure previously reported [21], with slightly larger lattice constants of $a = 6.5449(7)$ Å and $c = 7.0328(9)$ Å. The chemical compositions determined by the inductively coupled plasma spectroscopy are 0.97(1) and 3.03(1) for Cd and Cu, respectively, which are close to the stoichiometric values. Magnetization was measured in a Magnetic Property Measurement System MPMS3 (Quantum Design), and both magnetic torque and heat capacity were measured in a Physical Property Measurement System PPMS (Quantum Design).

III. RESULTS

A. Magnetic susceptibility

Magnetic susceptibilities measured in magnetic fields of 1 T along the a and c axes exhibit Curie-Weiss-type
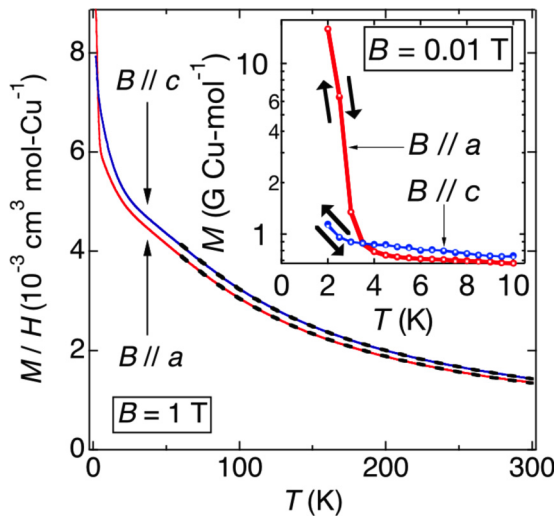
FIG. 4. Temperature dependence of magnetic susceptibilities from the one single crystal of CdK, the photograph of which is shown in Fig. 3(b). The measurements were carried out upon cooling in a magnetic field of 1 T applied along the a or c axis. The dashed lines on the data show fits to calculations by the high-temperature series expansion, which yields $J/k_B = 45.44(3)$ K. The inset shows magnetizations measured upon heating after zero-field cooling and then upon cooling below 10 K in a low field of 0.01 T.

temperature dependencies at high temperatures above ~ 100 K and a broad hump at ~ 30 K, followed by a further increase at low temperature, as shown in Fig. 4. The hump is probably due to a short-range antiferromagnetic correlation, and the low-temperature enhancement may be associated with a weak ferromagnetic correlation mentioned later. Linear extrapolations of the reciprocal susceptibility give Weiss temperatures of approximately -60 K for both the directions, which agree with the previous value from a polycrystalline sample [24]. The small anisotropy is attributed to a difference in the Landé g factor within the isotropic Heisenberg model. A simultaneous fit of the two data sets to the high-temperature series expansion for the $S = 1/2$ Heisenberg KAFM model [27] in the temperature range of 60–300 K (dotted lines in Fig. 4) yields $J/k_B = 45.44(3)$ K and $(g, \chi_0) = [2.2676(3), -3.62(7) \times 10^{-5}$ cm^{3}Cu $-$ mol$^{-1}]$ and $[2.3330(6), -2.76(8) \times 10^{-5}$ cm^3 Cu $-$ mol$^{-1}]$ for the a and c directions, respectively. The temperature-independent term χ_0 is from core diamagnetism (-6×10^{-5} cm^3 Cu-mol^{-1}) and Van Vleck paramagnetism (not known). The g values of CdK are along with typical values for Cu kagome minerals; $g = 2.1 \sim 2.2$ and $2.2 \sim 2.4$ for the parallel and perpendicular directions to the plane, respectively [28].

We also fitted the magnetic susceptibility data to the high-temperature series expansion for the J_1-J_2-J_d model employed to kapellasite [29]; an estimated set of J's for kapellasite are $J_1 = -12$ K, $J_2 = -4$ K, and $J_d = 15.6$ K, which seems to generate short-range correlations toward a cuboc2 type order [30]. Because of many parameters, however, a reliable set of the J values was not attained in our case. To be inferred safely from our fitting is that antiferromagnetic J_2 and ferromagnetic J_d are smaller than half of dominant antiferromagnetic J_1. Thus, a simple nearest-neighbor model
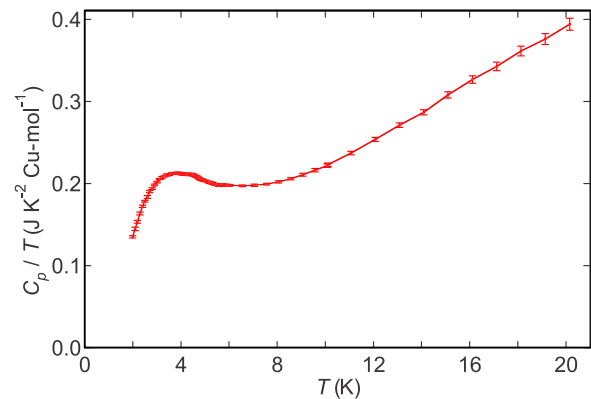

FIG. 5. Temperature dependence of heat capacity divided by temperature at zero magnetic field.

is a good starting point. The large differences in J_1 and J_d between CdK and kapellasite may come from differences in the bridging anions (Cl$^-$ for kapellasite and NO$_3{}^-$ for CdK) and deeper d levels of Cd than Zn.

B. Magnetic order

A distinct anisotropy in magnetic susceptibility appears below ~ 4 K, as shown in the inset to Fig. 4: the magnetization suddenly increases for $B \parallel a$, whereas remains less temperature dependent for $B \parallel c$. Corresponding to this anomaly in magnetization, heat capacity shows a broad peak at around 4 K, as shown in Fig. 5. These anomalies must indicate a long-range magnetic order at $T_N \sim 4$ K.

A possible reason why the heat capacity peak is so broad is an inhomogeneity associated with crystallographic disorder on the arrangement of the NO$_3{}^-$ unit [21]. Since one of the oxide ions of the NO$_3{}^-$ unit is located above or below the Cu triangle and mediates the nearest-neighbor superexchange coupling, this type of disorder may cause a spatial modulation in J. However, the disorder in CdK may not be strong enough to induce a spin-glass freezing as no differences were observed between zero-field and field-cooled magnetic susceptibility curves at small B (Fig. 4). On the other hand, there can be an additional or alternative reason for the broadening at the magnetic transition, which will be addressed later.

C. Weak ferromagnetism

Figure 6 shows magnetization processes at $T = 2$ K below T_N. Surprisingly, ferromagnetic behavior with a steep change near zero field is observed for $B \parallel a$ and $a - b$, whereas is completely absent for $B \parallel c$, implying that a ferromagnetic moment exists only within the kagome plane! This is in distinct contrast to the out-of-plane weak ferromagnetism observed in the Cr jarosite [31]. Subtracting a linear component obtained by fitting M in the range of 6–7 T from the M-B curve for $B \parallel a$ yields a small saturated magnetization of 7.93×10^{-3} μ_B/Cu, just 0.8% of the expected magnetic moment for $S = 1/2$; almost the same value for $B \parallel a - b$ indicates a weak anisotropy within the plane. A similar subtraction for $B \parallel c$ gives a residual magnetization well fitted by the $S = 1/2$ Brillouin function with a nearly equal saturation. This means
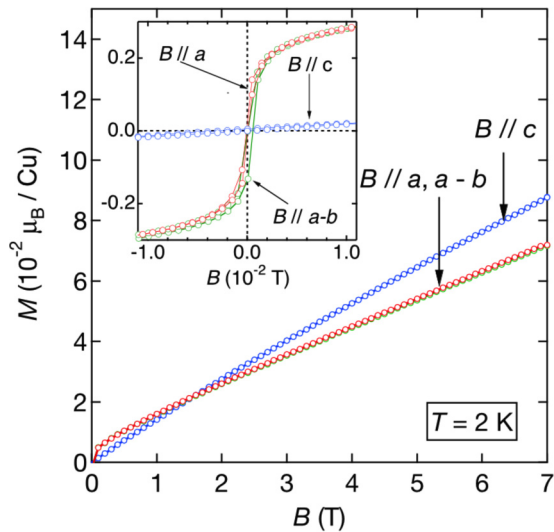
FIG. 6. Magnetization processes measured at 2 K. Blue, green, and red marks are data for $B \parallel c, a - b$, and a, respectively. The inset expands the small field range of $-0.02 \sim 0.02$ T.
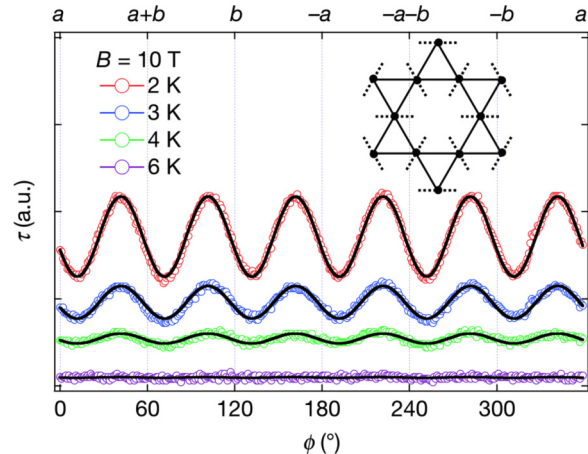

FIG. 7. Magnetic torque τ at various temperatures measured by rotating one crystal of CdK around the c axis in a magnetic field of 10 T. The rotation angle ϕ is set to zero at $B \parallel a$. The solid line on each data set is a fit to Eq. (2). Easy axes appear with $60°$ interval at $a, a + b, \ldots$, as indicated at the top of the panel. The inset depicts a kagome net with thus determined local easy axes shown by the broken lines.

that the weak ferromagnetic moment lying in the plane is forced to align by the perpendicular field.

Since this weak ferromagnetism is observed only below T_N and exhibits clear anisotropy, it should not originate from impurities, but must be parasitic to the antiferromagnetic order. Thus, it is plausible that a canted antiferromagnetic order is realized in CdK.

Alternative possibility is to ascribe such a small ferromagnetic moment to a magnetic domain wall (MDW). It was very recently found that uncompensated magnetic moments at MDWs in the three-dimensional all-in/all-out antiferromagnetic order of the pyrochlore oxide $Cd_2Os_2O_7$ give robust weak ferromagnetic moments [32]. Similar uncompensated moments at MDWs were observed in an oxalate compound with a PVC order on a distorted kagome net [17]. In this case, however, the uncompensated moments behave as uncorrelated quasifree moments at low temperature; it is unlikely that uncompensated moments at MDWs behave as correlated ferromagnetic moments in quasi-two-dimensional antiferromagnets. Therefore, we think it reasonable to assume that the weak ferromagnetism of CdK originates from a spin canting in the antiferromagnetic order.

D. Magnetic anisotropy

The magnetic anisotropy is relatively small in the kagome plane, as evidenced by the nearly equal M values for $B \parallel a$ and $a - c$ in Fig. 6. However, there must be a tiny anisotropy reflecting the crystal symmetry. To investigate this, magnetic torque τ was measured by rotating the crystal around the c axis in a magnetic field of 10 T. Torque curves with clear $60°$ periodicity appear below T_N and grow with decreasing temperature, as shown in Fig. 7.

The τ in the ab plane of a trigonal crystal system is given by Eq. (2):

$$E(\phi) = K \cos 6\phi, \quad \tau(\phi) = -\frac{\partial E}{\partial \phi} = K \sin 6\phi, \quad (2)$$

where ϕ is an angle from the easy or hard axis within the ab plane, and K is the magnetocrystalline anisotropy energy of the lowest order [33]. Since the experimental data are well reproduced by Eq. (2), the trigonal crystal symmetry is actually preserved down to 2 K; no structural symmetry lowering takes place at low temperature. In addition, easy axes are determined at angles where the derivative of the torque curve becomes minimum: they are [100] and its equivalent directions $\langle 100 \rangle$. As a result, the local easy axes point to the center of the hexagon of the kagome net, as depicted in the inset to Fig. 7. Note that the $a - b$ direction corresponds to $\phi = 330°$, which is found to be a hard axis in the torque curves. Since the difference in M between the easy and hard axes is negligible, the anisotropy energy within the plane is quite small.

IV. DISCUSSION

Summarizing our experimental results, CdK is a spin-1/2 Heisenberg KAFM with $J = 45$ K in the undistorted kagome net and exhibits a canted antiferromagnetic order accompanied by a weak ferromagnetic moment only within the kagome plane below $T_N = 4$ K. From the torque measurements, the easy axes are determined as $\langle 100 \rangle$. Now, we discuss the possible magnetic structure of CdK.

A. Dzyaloshinskii-Moriya interaction

Taking account of DM interactions, which should exist in the absence of inversion center at the middle of the bond between nearby Cu sites and must cause a spin canting as often observed in other KAFMs [34], we consider the spin Hamiltonian given by

$$H = \sum_{\overrightarrow{ij}} (J \, S_i \cdot S_j + D_{ij} \cdot S_i \times S_j), \quad (3)$$
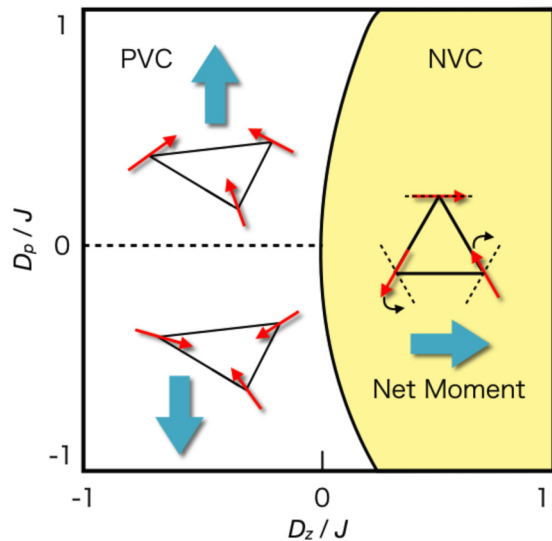
FIG. 8. Phase diagram for the ground state of the classical kagome antiferromagnet with the nearest-neighbor antiferromagnetic interaction J and DM interaction [36,37]. Negative and positive D_z tend to stabilize the PVC and NVC spin structures, respectively. In PVC, every spin is canted upward and downward by positive and negative D_p, respectively, keeping the threefold rotational symmetry. This causes an out-of-plane net magnetization shown by the thick arrow. In NVC, spins are mostly within the plane and the threefold rotational symmetry is broken. The dashed lines on the triangle represent $\langle 100 \rangle$ easy axes. When one of the three spins on the triangle is pinned along the easy axis, the other two spins are not, which can generate a small tilting and cause an in-plane net magnetization.

where D_{ij} is the DM vector between two sites i and j on the triangle; the convention is taken same as for the vector chirality in Eq. (1). In CdK, since there is a mirror plane perpendicular to the bond, the DM vector should be confined in the mirror plane as depicted in Fig. 2(b); D_z and D_p are set to represent the out-of-plane and in-plane components, respectively; following the same convention used for the vector chirality, positive D_z means a DM vector pointing upward from the paper in Fig. 2(b) [35].

The effects of the DM interaction on the classical KAFM have been theoretically studied, and a phase diagram of Fig. 8 is obtained by Monte Carlo simulations [36,37]. Upon switching the DM interaction, all the spins are forced to lie in the kagome plane so that such coplanar spin structures as shown in Fig. 1 are selected; D_z acts like an easy-plane anisotropy. Moreover, the $\mathbf{q} = 0$ structures become more stable than the SVC structure and appear at $T \sim |D|$ [36]. Importantly, the sign of D_z selects the PVC or NVC because it is explicitly coupled to the vector chirality in Eq. (1): PVC is favored for negative D_z, while NVC for positive D_z; the D_z term is canceled out for SVC. On the other hand, D_p tends to favor PVC so that large $|D_p|$ selects PVC even for positive D_z [37], which causes the phase boundary bent in Fig. 8. However, because $|D_p|$ and $|D_z|$ are often smaller than J in real materials, one concludes that the sign of D_z dominantly selects the spin structure.

In PVC, finite D_p renders all spins to cant from the plane to an umbrella structure and leads to a spontaneous magnetization parallel to the c axis [36]. This is not the case of CdK but of the Cr jarosite [31]. Note that D_p breaks

the in-plane rotational symmetry and may induce in-plane anisotropy along $\langle 1\bar{1}0 \rangle$, which is different from the observed anisotropy along $\langle 100 \rangle$ for CdK.

Considering only DM interaction as a source of anisotropy, the NVC structure preserves the degree of freedom of global spin rotation in the plane. Nevertheless, it can be broken by a higher-order anisotropy term, and an in-plane net moment can occur. For example, when there is a $\langle 100 \rangle$ easy-axis anisotropy, a net magnetization is produced as illustrated in Fig. 8: in every triangle, only one moment can be parallel to the local easy axis, but the other two cannot, which may cause a canting that generates an uncompensated moment in the plane. A candidate for this higher-order anisotropy term is an anisotropic symmetric exchange interaction, which is usually much smaller than DM interactions [38].

Provided that the magnetic moment is $1 \mu_B$/Cu, the spin rotation angle necessary to produce the observed weak ferromagnetic moment of $0.008 \mu_B$/Cu is calculated to be as small as $0.6°$. This tiny value suggests that the higher-order anisotropy energy is much smaller than J which favors a $120°$ structure. This is also the reason for the indiscernible hysteresis in the magnetization curves of Fig. 6.

The above discussion is valid for classical KAFMs. However, as Cepas and co-workers show, a quantum KAFM takes a $\mathbf{q} = 0$ order for $|D_z|/J > 0.1$ [10]. The magnitude of D for CdK is roughly estimated by $(\Delta g/g)J \sim 0.1J$ [38], suggesting that CdK exists close to the boundary and probably in the ordered side. This value is also consistent with $T_N \sim |D| \sim 4$ K. Once a $\mathbf{q} = 0$ order sets in, the above classical arguments must be applied; quantum effects manifest themselves only in the contraction of a magnetic moment. Therefore, it is plausible to assume that the magnetic structure of CdK is NVC. Note that the presence of sizable DM interaction and the in-plane spontaneous magnetization strictly exclude SVC and PVC structures, and the observed easy axis of $\langle 100 \rangle$ is compatible with the NVC. Moreover, other coplanar or noncoplanar complex spin structures must not give such a weak ferromagnetism with distinct anisotropy.

The origin of the NVC order in CdK is apparently ascribed to the positive D_z, which happens to occur by the microscopic details of the compound [36]. On one hand, a similar NVC order has been established in the three-dimensional, metallic compounds, Mn_3Sn and Mn_3Ge, which contain a stack of "breathing" kagome nets of Mn moments of $\sim 3 \mu_B$ [39]. Recently, they attract much attention because of the large anomalous Hall effects even in the antiferromagnets [9,40,41]. Probably, the better two dimensionality and simpler magnetic interactions make CdK an optimized prototype of the NVC order.

B. Representation analysis

To support the above discussion, particularly on the direction of the weak ferromagnetic moment, a representation analysis has been carried out using the program SARA h developed by Wills for representational analysis [42]; these results are basically same as the previous analysis for the jarosites [43]. The following implications are obtained:

(1) Twelve symmetry elements in the space group of $P-3m1$ make the propagation vector $\mathbf{k} = (0,0,0)$ invariant. The magnetic representation of a crystallographic site at

TABLE I. Irreducible representations (IRs) and basis vectors (BVs) for the space group $P-3m1$ with $\mathbf{k} = (0,0,0)$. The decomposition of the magnetic structure representation for the $3e$ site (1/2, 0, 0) is $\Gamma_{\text{mag}} = \Gamma_1 + \Gamma_3 + 3\Gamma_6^2$. The atoms in the nonprimitive basis are defined as 1 (1/2, 0, 0), 2 (0, 1/2, 0), and 3 (1/2, 1/2, 0). The BV components along the crystallographic axes are shown by m_i ($i = a,b,c$).

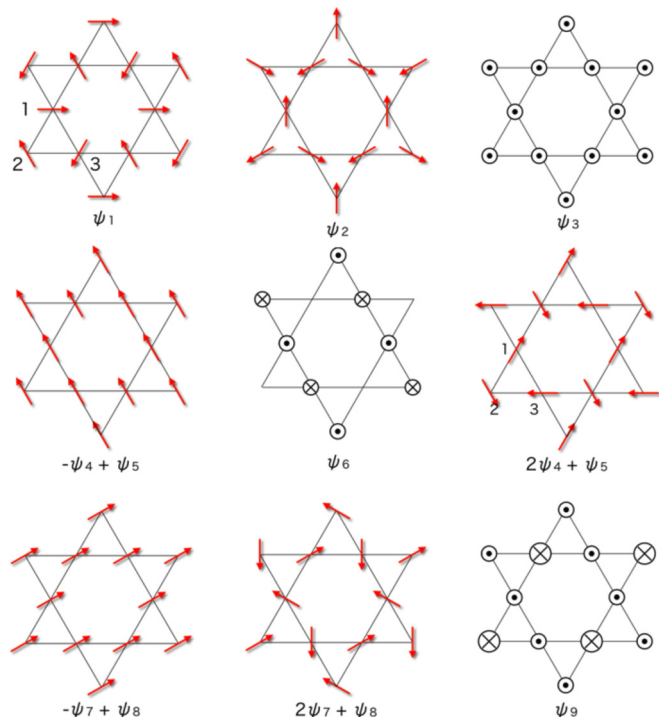| IR	BV	Atom	BV components		
			m_a	m_b	m_c
Γ_1	ψ_1	1	4	0	0
		2	0	4	0
		3	−4	−4	0
Γ_2	ψ_2	1	2	3	0
		2	−4	−2	0
		3	2	−2	0
	ψ_3	1	0	0	4
		2	0	0	4
		3	0	0	4
Γ_3	ψ_4	1	1	0	0
		2	0	−2	0
		3	−1	−1	0
	ψ_5	1	1	3	0
		2	0	1	0
		3	−1	2	0
	ψ_6	1	0	0	3
		2	0	0	0
		3	0	0	−3
	ψ_7	1	$-\sqrt{3}$	0	0
		2	0	0	0
		3	$-\sqrt{3}$	$-\sqrt{3}$	0
	ψ_8	1	$\sqrt{3}$	$\sqrt{3}$	0
		2	$2\sqrt{3}$	$\sqrt{3}$	0
		3	$\sqrt{3}$	0	0
	ψ_9	1	0	0	$\sqrt{3}$
		2	0	0	$-2\sqrt{3}$
		3	0	0	$\sqrt{3}$

FIG. 9. Schematic representation of basis vectors for the space group $P-3m1$ with $\mathbf{k} = (0,0,0)$. A spin on each lattice point is represented by an arrow when it is confined in the plane, and by a circle when it is perpendicular to the plane. In ψ_9 one large downward spin and two small upward spins in the triangle cancel with each other.

(1/2, 0, 0) can be decomposed into irreducible representations of $\Gamma_1 + 2\Gamma_3 + 3\Gamma_6^2$, which basis vectors are listed in Table I. Nine possible spin arrangements are schematically shown in Fig. 9. The PVC orders with $\langle 100 \rangle$ and $\langle 1\bar{1}0 \rangle$ anisotropies belong to Γ_1 (ψ_1) and Γ_3 (ψ_2), respectively, and the NVC order belongs to Γ_6 ($2\psi_7 + \psi_8$).

(2) For PVC, only out-of-plane weak ferromagnetism is allowed for $\langle 1\bar{1}0 \rangle$ anisotropy by combining ψ_2 with ψ_3 having a ferromagnetic spin arrangement along c in Γ_3. In contrast, such a canting is not allowed for $\langle 100 \rangle$ anisotropy in Γ_1.

(3) For NVC, in-plane weak ferromagnetism is allowed because there is an in-plane ferromagnetic configuration in Γ_6; $-\psi_4 + \psi_5$ or $-\psi_7 + \psi_8$. A spin canting along c is also possible, but no net moment should appear as there is no basis vector with a net moment along c in Γ_6; all the spins in ψ_9 cancel with each other.

(4) Six symmetry elements make the propagation vector $\mathbf{k} = (1/3, 1/3, 0)$ invariant in the subgroup $G_{\mathbf{q}}$ of $P-3m1$. If

symmetry elements are restricted to ones in $G_{\mathbf{q}}$, the situation is same as for Γ_6 in $\mathbf{k} = (0,0,0)$. Thus, a weak in-plane ferromagnetic moment is also allowed in SVC.

According to the representation analysis, the appearance of weak ferromagnetic moments only in the plane is not consistent with the PVC order but with either the NVC or the SVC order. Although the possibility of an SVC order is not excluded, finite DM interactions may prefer a NVC order in CdK, as mentioned above.

C. Critical phenomenon

Finally, we point out one intriguing feature of the NVC order with $\langle 100 \rangle$ anisotropy as realized in CdK and its relation to the broad peak in the heat capacity at the transition. The canted NVC structure or any magnetic structure with spin canting that causes an in-plane weak ferromagnetic moment spontaneously breaks Z_6 anisotropy. In three dimensions, numerical calculations on the XY model with Z_6 anisotropy suggest that the critical phenomena belong to the 3D XY universality class [44–46]. Interestingly, this type of critical behavior may be closely related to the "deconfined" quantum criticality [47–49]. Thus, it would be interesting to investigate the critical behavior of the transition to NVC that breaks the Z_6 symmetry in CdK. One implication to experiments is that the transition may not be accompanied by a divergence in heat capacity. The observed broad peak in the heat capacity of CdK is possibly intrinsic and may be related to the unique characteristics of the transition to NVC.

V. CONCLUSION

We have successfully grown single crystals of the kagome antiferromagnet $CdCu_3(OH)_6(NO_3)_2 \cdot H_2O$ with $J = 45$ K, and suggest a NVC spin order below $T_N \sim 4$ K. The origin of the NVC order is considered to be a DM interaction with a positive z component. We believe that there are novel phenomena for this NVC order to be searched for in the future work.

ACKNOWLEDGMENTS

[1] J. N. Reimers and A. J. Berlinsky, Phys. Rev. B **48**, 9539 (1993).

[2] D. A. Huse and A. D. Rutenberg, Phys. Rev. B **45**, 7536(R) (1992).

[3] J. T. Chalker, P. C. W. Holdsworth, and E. F. Shender, Phys. Rev. Lett. **68**, 855 (1992).

[4] A. B. Harris, C. Kallin, and A. J. Berlinsky, Phys. Rev. B **45**, 2899 (1992).

[5] S. Yan, D. A. Huse, and S. R. White, Science **332**, 1173 (2011).

[6] Y. Iqbal, F. Becca, S. Sorella, and D. Poilblanc, Phys. Rev. B **87**, 060405(R) (2013).

[7] M. Pereiro, D. Yudin, J. Chico, C. Etz, O. Eriksson, and A. Bergman, Nat. Commun. **5**, 4815 (2014).

[8] H. Chen, Q. Niu, and A. H. MacDonald, Phys. Rev. Lett. **112**, 017205 (2014).

[9] S. Nakatsuji, N. Kiyohara, and T. Higo, Nature (London) **527**, 212 (2015).

[10] O. Cépas, C. M. Fong, P. W. Leung, and C. Lhuillier, Phys. Rev. B **78**, 140405(R) (2008).

[11] J. C. Domenge, P. Sindzingre, C. Lhuillier, and L. Pierre, Phys. Rev. B **72**, 024433 (2005).

[12] T. Inami, S. Maegawa, and M. Takano, J. Magn. Magn. Mater. **177-181**, 752 (1998).

[13] D. Grohol, K. Matan, J.-H. Cho, S.-H. Lee, J. W. Lynn, and D. G. Nocera, Nat. Mater. **4**, 323 (2005).

[14] Y. Okamoto, H. Yoshida, and Z. Hiroi, J. Phys. Soc. Jpn. **78**, 033701 (2009).

[15] M. Yoshida, Y Okamoto, M. Takigawa, and Z. Hiroi, J. Phys. Soc. Jpn. **82**, 013702 (2012).

[16] H. Yoshida, Y. Michiue, E. Takyama-Muromachi, and M. Isobe, J. Mater. Chem. **22**, 18793 (2012).

[17] E. Lhotel, V. Simonet, J. Ortloff, B. Canals, C. Paulsen, E. Suard, T. Hansen, D. J. Price, P. T. Wood, A. K. Powell, and R. Ballou, Phys. Rev. Lett. **107**, 257205 (2011).

[18] M. P. Shores, E. A. Nytko, B. M. Bartlett, and D. G. Nocera, J. Am. Chem. Soc. **127**, 13462 (2005).

[19] M. Fu, T. Imai, T.-H. Han, and Y. S. Lee, Science **350**, 655 (2015).

[20] D. P. Kozlenko, A. F. Kusmartseva, E. V. Lukin, D. A. Keen, W. G. Marshall, M. A. de Vries, and K. V. Kamenev, Phys. Rev. Lett. **108**, 187207 (2012).

[21] H. R. Oswald, Helv. Chim. Acta. **52**, 2369 (1969).

[22] W. Krause, H.-J. Bernhardt, R. S. W. Braithwaite, U. Kolitsch, and R. Pritchard, Mineral. Mag. **70**, 329 (2006).

[23] E. A. Nytko, M. P. Shores, J. S. Helton, and D. G. Nocera, Inorg. Chem. **48**, 7782 (2009).

[24] Y. Okamoto, M. Yoshida, H. Ishikawa, G. J. Nilsen, H. Yoshida, and Z. Hiroi, presented at International Conference on Magnetism, Busan, Korea, 2012 (unpublished).

[25] R. H. Colman, A. Sinclair, and A. S. Wills, Chem. Mater. **22**, 5774 (2010).

[26] S. Chu, P. Müller, D. G. Nocera, and Y. S. Lee, Appl. Phys. Lett. **98**, 092508 (2011).

[27] N. Elstner and A. P. Young, Phys. Rev. B **50**, 6871 (1994).

[28] A. Zorko, S. Nellutla, J. van Tol, L. C. Brunel, F. Bert, F. Duc, J.-C. Trombe, M. A. de Vries, A. Harrison, and P. Mendels, Phys. Rev. Lett. **101**, 026405 (2008).

[29] B. Bernu, C. Lhuillier, E. Kermarrec, F. Bert, P. Mendels, R. H. Colman, and A. S. Wills, Phys. Rev. B **87**, 155107 (2013).

[30] B. Fåk, E. Kermarrec, L. Messio, B. Bernu, C. Lhuillier, F. Bert, P. Mendels, B. Koteswararao, F. Bouquet, J. Ollivier, A. D. Hillier, A. Amato, R. H. Colman, and A. S. Wills, Phys. Rev. Lett. **109**, 037208 (2012).

[31] K. Okuta, S. Hara, H. Sato, Y. Narumi, and K. Kindo, J. Phys. Soc. Jpn. **80**, 063703 (2011).

[32] Hishiro T. Hirose, Jun-ichi Yamaura, and Zenji Hiroi, Sci. Rep. **7**, 42440 (2017).

[33] L. D. Landau, E. M. Lifshitz, and L. P. Pitaevskii, *Electrodynamics of Continuous Media*, Vol. 8 (Elsevier, Amsterdam, 1984).

[34] T. Yildirim and A. B. Harris, Phys. Rev. B **73**, 214446 (2006).

[35] For the definition of both the vector chirality and the DM interactions, the rotation of sites in the triangle is always set counterclockwise for every triangle in this study. Note that the three DM vectors in a triangle are related by the threefold rotation axis in the center of gravity of the triangle. Between adjacent triangles the DM vector does not change its direction by the space inversion at the connecting Cu site, because it is an axial vector. In many previous studies, however, the same notation was used for the vector chirality, while another notation was applied for the DM interaction, in which counterclockwise and clockwise rotations of sites are assumed alternatingly, resulting in the flipping of the DM vectors between adjacent triangles. We would like to avoid confusion by using the two kinds of notation.

[36] M. Elhajal, B. Canals, and C. Lacroix, Phys. Rev. B **66**, 014422 (2002).

[37] The convention assumed in Ref. [36] is that the spins in the cross products of the DM interaction appear rotating counterclockwise around the hexagon, i.e., clockwise in the triangle. In this paper, following the more general convention, we take it counterclockwise in the triangle. As the result, the sign of D_z is reversed compared with the original work.

[38] T. Moriya, Phys. Rev. **120**, 91 (1960).

[39] T. Nagamiya, S. Tomiyoshi, and Y. Yamaguchi, Solid State Commun. **42**, 385 (1982).

[40] Ajaya K. Nayak, J. E. Fischer, Y. Sun, B. Yan, J. Karel, A. C. Komarek, C. Shekhar, N. Kumar, W. Schnelle, J. Kübler, C. Felser, and S. S. P. Parkin, Sci. Adv. **2**, e1501870 (2016).

[41] In the study on these compounds, other terms such as a "triangular spin configuration with negative1 chirality" or "inverse triangular spin structure" are used instead of our NVC spin structure.

[42] A. S. Wills, Phys. B (Amsterdam) **276-278**, 680 (2000).

[43] A. S. Wills, Phys. Rev. B **63**, 064430 (2001).

[44] S. Miyashita, J. Phys. Soc. Jpn. **66**, 3411 (1997).

[45] M. Oshikawa, Phys. Rev. B **61**, 3430 (2000).

[46] T. Okubo, K. Oshikawa, H. Watanabe, and N. Kawashima, Phys. Rev. B **91**, 174417 (2015).

[47] T. Senthil, A. Vishwanath, L. Balents, S. Sachdev, and M. P. A. Fisher, Science **303**, 1490 (2004).

[48] P. Kroll, Phys. Rev. B **72**, 144407 (2005).

[49] H. Shao, W. Guo, and A. W. Sandvik, Science **352**, 213 (2016).